Journal of Material Cycles and Waste Management (2024) 26:882–893
https://doi.org/10.1007/s10163-023-01865-8

ORIGINAL ARTICLE

Synthesis of highly basic, low-cost iron oxides from tin can waste as valorization of municipal solid waste and study of their catalytic efficiency as potent catalysts for MEK production

Abouelhassan A. Gomaa[1] · Ahmed I. Osman[2] · Samih A. Halawy[1] · Mohamed A. Mohamed[1] · Adel Abdelkader[1]

Received: 14 January 2023 / Accepted: 15 November 2023 / Published online: 26 December 2023

Abstract

In the present study, low-cost iron oxide catalysts have been prepared by a simple precipitation method using tin food can waste as a source of iron and sodium hydroxide or ammonium hydroxide solution as a precipitating agent. The prepared catalysts were characterized by thermogravimetric analysis (TGA), differential thermal analysis (DTA), X-ray diffraction (XRD), FT-IR spectra, scanning electron microscopy (SEM), EDAX quantitative elemental analysis, and BET surface area measurements. Surface basicity of iron oxide catalysts was measured by adsorption of carbon dioxide as an acidic probe molecule, followed by desorption measurements using the TGA technique. The prepared iron oxide catalysts were tested by dehydrogenation of 2-butanol to methyl ethyl ketone (MEK) at a temperature range of 275–375 °C. Commercial iron oxide was tested under identical reaction conditions for comparison with the prepared catalysts. The results indicated the superiority of the prepared catalysts over the commercial one and the superiority of the catalyst prepared using NaOH over that prepared using NH_4OH as precipitating agents. The use of different precipitating agents affects the surface morphology and, consequently, the catalytic activity of the produced iron oxide catalysts.

Graphical abstract

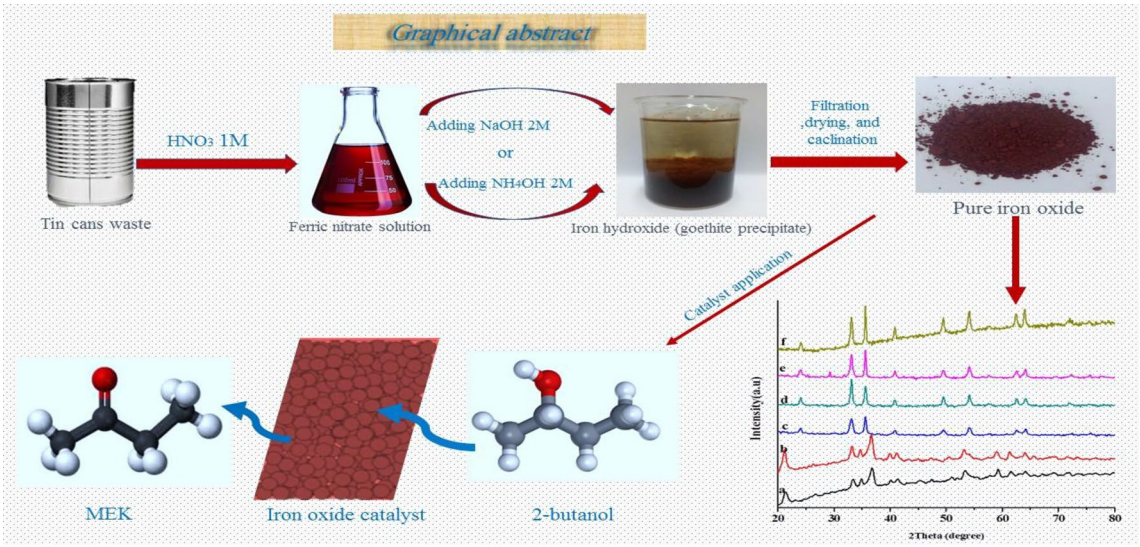

Keywords Tin can waste · Iron oxide · 2-Butanol · MEK · Dehydrogenation reaction

Extended author information available on the last page of the article

Introduction

The benefits from resources and the achievement of self-sufficiency in all aspects are one of the most important requirements for all countries in the current period. Two of the most important topics in this regard, which this paper link together, are the valorization of municipal solid waste (MSW) and the production of fossil fuel alternatives. Continuous population growth and urban development has led to a high level of MSW generation. MSW represents a national wealth when utilized in the right ways and a disaster when neglected. In addition, the high population and high living standards have led to a high rate of energy consumption which makes it necessary to look for alternatives to fossil fuel, especially in non-petroleum countries.

The amount of MSW generated worldwide every year is about 2 billion tons and it is expected to increase to about 3.4 billion tons by 2050 [1, 2]. The composition of the MSW depends on many factors including country, people's income, lifestyle/culture, climate, energy sources, etc. [3, 4]. The MSW in developing countries is mostly organic in nature including food scraps, wood, leaves, and process residues from farms, while the MSW in developed countries is mainly inorganic in nature such as plastic, paper, metal, and e-wastes [3]. In general, MSW includes kitchen waste, agriculture waste, metals, paper, glass, plastic, electronic waste, inert materials, and miscellaneous thrash [1, 5]. The treatment approaches of the MSW worldwide include landfilling, which ends up at about 70% of the produced MSW, in addition to classified recycling, incineration, pyrolysis, gasification, composting, and anaerobic digestion [1, 6, 7]. All these approaches represent a threat to the environment and human health in one way or another. For example, these approaches pose potential risks of infection in the case of manual sorting of MSW or explosion in the case of landfilling, incineration, pyrolysis, gasification, or anaerobic digestion [7]. Therefore, it is necessary to develop effective approaches to utilize these waste materials as valuable resources, in alignment with the principles of sustainability and environmental preservation. The metallic/metal-containing waste is one of the most important categories of MSW. The proper utilization of this kind of waste needs to be thoroughly examined to conserve natural resources, particularly, considering that these metals represent non-renewable resources. There are many studies in the literature that have investigated the valorization of different kinds of metallic/metal-containing MSW. Liu et al. [8] presented a novel and effective smelting–-collection process for recovering platinum from waste automotive catalysts (WAC). The process involves mixing different WAC carriers (cordierite and alumina), adding iron powder as a collector metal, and CaO as a flux agent. By optimizing the process conditions, a platinum recovery rate of over 98% was achieved. The recovered platinum was concentrated into Fe–Pt alloy, and environmentally safe glass slag was obtained. Marinato et al. [9] achieved a 98.4% silver recovery from waste printed circuit boards of obsolete cell phones through hydrometallurgical processing. The recovered silver was converted to silver chloride and used for green synthesis of silver nanoparticles which exhibited strong antibacterial properties against Gram-negative bacteria, particularly, *Escherichia coli*. Wang et al. [10] studied the recovery of high-purity metallic cobalt from NMC-type Li-ion batteries, utilizing lithium nickel manganese cobalt oxide as the cathode material. The recovery process involves the reductive acidic leaching of the cathode material, followed by selective extraction of cobalt. The overall recovery ratio for cobalt was calculated at approximately 93%, with a remarkably high purity of 98.8%. In a study by Roy et al. [11], a simple and facile strategy was applied to convert waste aluminum cans to nano-alumina which was used as reinforcing filler for the development of natural rubber composites with balanced compact performances. According to Roy and his co-workers, addition of the can waste-based nano-alumina successfully enhances the thermal stability and thermal oxidative aging resistance of natural rubber composites. Tin food packaging cans, primarily composed of iron with a small tin content, constitute a significant portion of the metal category in municipal solid waste (MSW). Tin can waste is generated in a daily basis worldwide due to their extensive use in packaging various food items, particularly low-cost food products. In 2003, the worldwide production of tin cans for food packaging was estimated to be about 80,000 million cans [12]. Despite the substantial production of this iron-based waste, the studies on the utilization of tin cans waste are limited compared to other types of metal waste. This may be attributed to the abundance of iron as an element, its multiple natural sources, and its cost-effectiveness compared to other metals. However, despite these factors, it is important from the environmental and economical points of view to give the management of iron waste more attention.

Many fossil fuel alternatives have captured the attention of researchers nowadays, and there is hope that these alternatives will contribute to solving the energy problem. Methyl ethyl ketone or 2-butanone C_4H_8O is suggested to be used as a possible fuel for spark-ignition engines and is considered one of the promising alternative energy sources that can contribute significantly to reducing dependence on fossil fuel [13]. It is an extremely volatile and flammable colorless liquid with a sharp, sweet odor like that of butterscotch and acetone [14, 15]. MEK has many important industrial applications, including the production of paints, lacquers, varnishes, sticks, resins, gums, nitrocellulose,

cells, and artificial leather. In addition, MEK is used in the printing industry and in the manufacture of dyes and as an aerosol surface cleaner [14]. In general, the production of MEK can be carried out by two routes, first route through compounds produced by oil refining, and the second route which involves intermediate compounds recovered from biomass by biological methods [14]. In addition, MEK can be produced directly by fermentation of biomass; however, the yields of this process are quite low [13]. The industrial process to produce MEK is performed through the dehydrogenation of 2-butanol, the alcohol which can be produced by chemical routes from fossil fuel or biologically from biomass fermentation [13, 16]. The most common catalysts employed for dehydrogenation of 2-butanol to MEK are copper-based catalysts and/or zinc-based catalysts [17]. Additionally, many different catalytic systems have been studied for the dehydrogenation of alcohols in general including Cu–Ce–Zr-based catalysts, Cu–Ni bimetallic catalysts supported on gamma alumina, Pt supported on different oxides, and solid-state molybdenum sulfide clusters [18]. Geravand et al. [15] studied the vapor-phase dehydrogenation of 2-butanol to MEK at 260 °C using Cu/ZnO/Al_2O_3 and Cu/SiO_2 nanocatalysts prepared by three different methods: impregnation, sol–gel, and co-precipitation. They found that the activity and MEK selectivity of the prepared catalysts increased in the following sequence: CuO/ZnO/Al_2O_3 (co-precipitation) > CuO/SiO_2 (sol–gel) > CuO/SiO_2 (impregnation). In addition, the optimum preparation conditions of the catalyst CuO/ZnO/Al_2O_3 (co-precipitation) that can maximize MEK selectivity, according to this study, are precipitation temperature of 67.5 °C, aging temperature of 68.75 °C, pH of precipitation stage of 7.27 and Cu/Zn molar ratio of 1.38. Zhanga et al. [19] studied the dehydrogenation reaction of 2-butanol to MEK over copper and zinc catalysts supported on Al_2O_3–ZrO_2 composite carriers prepared by the co-precipitation method. They investigated the effect of Al/Zr ratio on the catalytic performance and found that the addition of an appropriate amount of Zr component to the CuO–ZnO–Al_2O_3 catalyst helped disperse CuO species, lower its reduction temperature, and improve its reduction characteristics. According to this study, 2-butanol conversion of 95% and MEK selectivity of 78% was obtained when the CuO:ZnO:Al_2O_3:ZrO_2 molar ratio was 1:1:0.06:0.5 at a reaction temperature of 230 °C. Halawy et al. [20] studied the production of MEK through the dehydrogenation of 2-butanol over nanocrystalline NiO catalyst with a coral-like structure (38 nm) prepared by the thermal decomposition of nickel galactarate ($NiC_6H_8O_8 \cdot 2H_2O$). The prepared NiO catalyst exhibited excellent catalytic activity in the synthesis of MEK from 2-butanol which was attributed to the distribution of strong basic sites on the catalyst surface. At a reaction temperature of 300 °C, the catalyst achieved 90% conversion of 2-butanol to MEK with a selectivity of 90%.

The aim of this study is to achieve two important objectives. The first objective is to benefit from tin can waste as a category of MSW, which, despite its large quantities, has not received sufficient attention from researchers compared to other types of MSW. This objective has been achieved by converting tin can waste to catalytically active iron oxide by applying a simple, low-cost precipitation method in which sodium hydroxide or ammonium hydroxide was used as precipitating agents after dissolving the cans in nitric acid. The second objective is to study the dehydrogenation of 2-butanol to MEK over the prepared iron oxide catalysts as a cost-effective alternative to the common catalysts used in this reaction in the industry. In general, iron oxide is a type of transition metal oxide which exists in different stoichiometric and crystalline forms, including wüstite (FeO), hematite (α-Fe_2O_3), maghemite (ν-Fe_2O_3), and magnetite (Fe_3O_4). Iron oxides have a wide range of applications in different fields, such as catalysis, photocatalysis, color imaging, magneto-optical devices, and ferro-fluids. Among all iron oxide phases, hematite (α-Fe_2O_3) is the most stable state under normal conditions and the most favored one due to its beneficial properties, chemical stability, and semiconducting characteristics [21].

Since the preliminary results showed the preference of the catalysts prepared using NaOH as a precipitating agent, the effect of calcination temperature on the morphological and catalytic properties of this catalyst has been studied. In addition, the catalytic efficiency of the produced iron oxide catalysts was compared with that of a commercial iron oxide catalyst.

Experimental

Materials

Waste tin food cans used in this study are those used in packing cooked fava beans and were collected from the local Egyptian market. All the chemicals were used in the condition as received without any further purification. These chemicals included nitric acid (HNO_3, Merck, 55%), ammonium hydroxide (NH_4OH, Merck, 35%), sodium hydroxide (NaOH, Merck), commercial hematite (Fe_2O_3, Merck), and 2-butanol ($CH_3CH(OH)CH_2CH_3$, Fluka).

Preparation of Fe_2O_3 catalysts from tin food can waste

Ferric nitrate solution was first prepared from food cans waste. 25 g of clean cans was cut to small pieces and immersed in a beaker containing 1000 mL of 1 M HNO_3 solution. The mixture was stirred till complete dissolution of the solid material; then the solution was filtered to remove

any insoluble materials. 200 mL of the filtrate was diluted to 600 mL using distilled water and heated to 100 °C, then 2 M NaOH solution was added dropwise with continuous stirring. The reddish-brown precipitate formed was stirred in the mother solution for 12 h at room temperature (pH of the mother solution was 11.2) and then filtered and washed several times with distilled water. The washed precipitate was dried at 100 °C for 24 h and finally calcined in static air for 3 h at 400 °C or higher temperatures. These steps were repeated using another 200 mL of the filtrate and 2 M NH_4OH solution as a precipitating agent (pH of the mother solution was 8.18). The sample prepared using NaOH was abbreviated as FeNa and that prepared using NH_4OH was abbreviated as FeNH, followed by the drying or calcination temperature, e.g., FeNa100, FeNa400, FeNH100, FeNH400, etc. Commercial Fe_2O_3 sample was used as a reference catalyst and was abbreviated as FeCm.

Catalyst characterization

Thermogravimetry (TG) was performed in a flow of 40 cm^3/min dry nitrogen, using automatically recording model 50 H Shimadzu thermal analyzer from Japan. The thermal analyzer is equipped with a data acquisition and handling system (TA-50WSI). FT-IR spectra of the samples were recorded using a Magna-FT-IR 500 from USA, in the range of 4000–300 cm^{-1}, operating a Nicolet Omnic software, and adopting the KBr disk technique. X-ray powder diffraction analysis (XRD) was carried out using a model D5000 Siemens diffractometer from Germany, equipped with a copper anode generating Ni-filtered Cu Kα radiation ($\lambda = 1.5406$ Å), in the 2θ range between 20° and 80°. An online data acquisition and handling system facilitated an automatic JCPDS library search and match using Diffrac software from Siemens for phase identification purposes. The BET surface area measurements were performed at liquid nitrogen temperature of −195 °C using an automatic Gemini VII Micromeritics Model 2390 P from USA. The catalyst samples were outgassed at 200 °C for 1 h prior to measurements. Scanning electron microscopy (SEM) was used to analyze the morphology of the samples using a JEOL JSM-IT200 SEM. The EDXRF quantitative elemental analysis was carried out using a Jeol JSX-3222 element analyzer system equipped with X-ray tube of Rh anode. The characteristic X-ray radiation was measured using a Si(Li) detector with an energy resolution of 149 eV at 5.9 keV and 1000 cps.

Determination of the surface basicity of the catalysts

The surface basicity of all the samples under investigation was studied quantitatively by means of desorption thermogravimetry using CO_2 as a probe molecule. 50 mg of each sample was pre-heated at 400 °C for 1 h in static air, then all the samples were kept for 2 weeks in a glass chamber fitted with a gas inlet and outlet under a flow of 40 mL/min CO_2 gas. 15–20 mg of sample covered with adsorbed CO_2 was subjected to TG analysis on heating up to 400 °C at a heating rate of 20 °C/min. The mass loss from TG analysis due to desorption of CO_2 molecules from the basic sites was determined as a function of surface basic sites density. Calculation of the density of the basic sites expressed in (site/g) was carried out using the following equation [22]:

$$\text{Basic site density (site/g)} = \frac{\text{Moles of } CO_2 \text{ desorped} \times \text{Avogadro Number (site/mol)}}{\text{Weight of sample } (g)}. \quad (1)$$

Catalytic activity measurements

The catalytic activity of all the catalysts for the vapor-phase dehydrogenation/dehydration of 2-butanol was performed in a continuous flow system under atmospheric pressure. The reactions were carried out in Pyrex glass reactor (1 cm wide and 16.5 cm long) using nitrogen as a carrier gas. 200 mg of the catalyst was preheated for 1 h at 400 °C under a flow of 100 mL/min nitrogen; then, the temperature was lowered to the reaction temperature, and the catalyst was subjected to the reaction feed (100 mL/min = 0.789% secondary butanol + 99.211% nitrogen). The reactor effluent was analyzed by using a gas chromatograph (Shimadzu GC-14A) equipped with a data processor model Shimadzu chromatopac C-R4AD (Japan). A flame ionization detector (FID) and a stainless-steel column (PEG 20M 20% on chromosorb W, 60/80 mesh, 3 m × 3 mm) at 80 °C were used to identify secondary butanol and the reaction products. Automatic sampling was performed with a heated gas sample cock, type HGS-2 at 140 °C.

Result and discussion

Catalyst characterization

Figure 1a, b shows the XRD and FT-IR analysis, respectively, of the dried precipitates, i.e., FeNa100 and FeNH100. From Fig. 1a, it can be seen that the two samples correspond to goethite (α-FeOOH) (JCPDS No 29-713), with its characteristic XRD peaks at 21°, 33°, 34°, 36°, 39°, 41°, 45°, 47°, 50°, 53°, 59°, 61°, and 64° [23, 24]. The peaks in Fig. 1a look rather sharp, indicating that these two samples have good crystallinity. Figure 1b shows the FT-IR spectra of FeNa100 and FeNH100 samples. In the two spectra, the IR bands at 798, 890 cm^{-1} can be ascribed to the (Fe–O–OH) bending vibration in goethite (α-FeOOH),

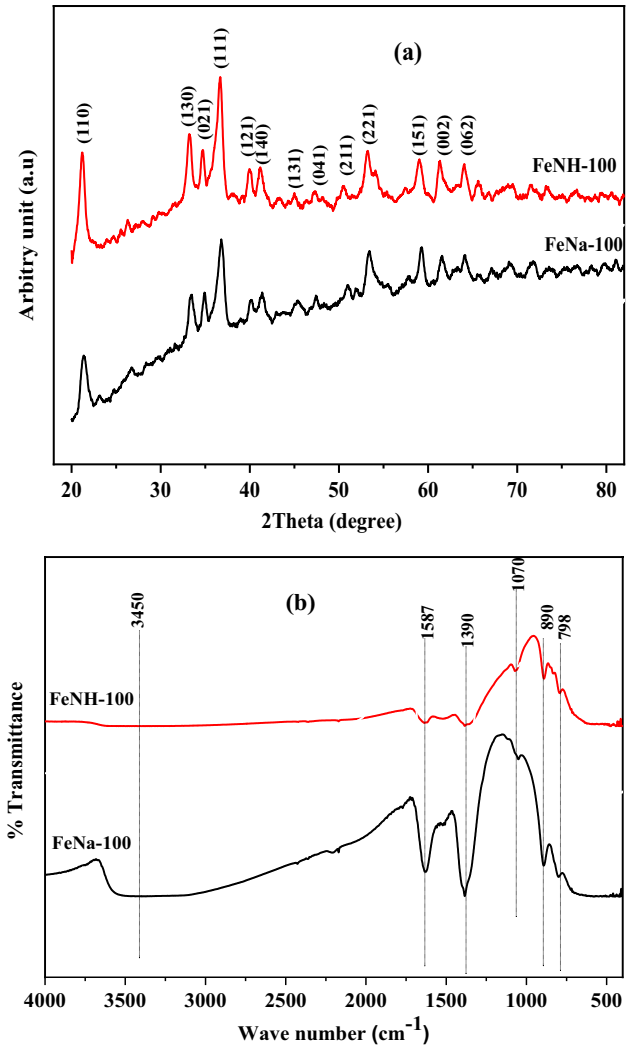

Fig. 1 XRD diffractograms (**a**) and FT-IR spectra (**b**) of the two parent materials FeNa100 and FeNH100 samples before calcination

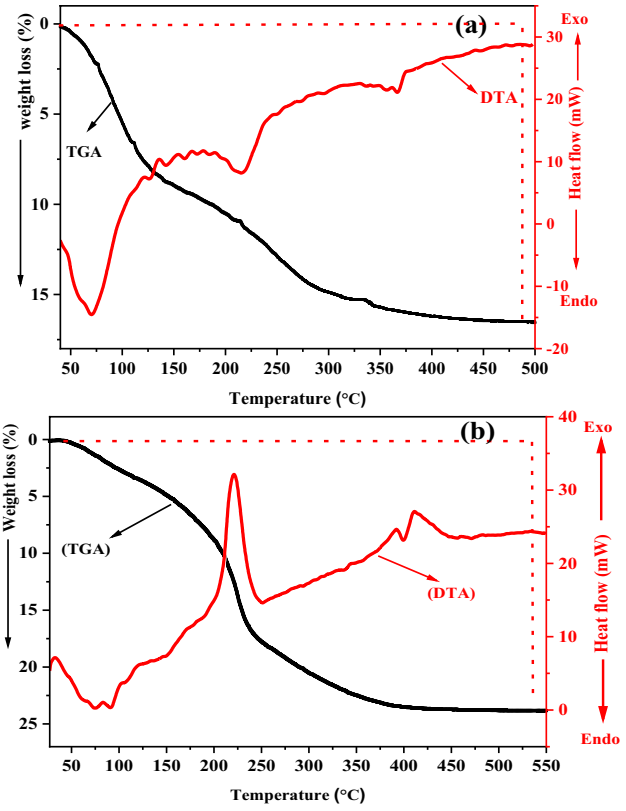

Fig. 2 TGA–DTA analysis of two parent materials, FeNa100 (**a**) and FeNH100 (**b**) performed in 40 mL/min dry N_2 with 10 °C /min heating rate

while bands at 1070, 1390, and 1587 cm^{-1} are likely due to carbonate groups of the adsorbed carbon dioxide from atmosphere [25, 26]. The intensity of the two bands at 1390 and 1587 cm^{-1} corresponding to carbonate groups is much higher in the case of FeNa100 than FeNH100, which indicates the higher surface basicity of the first one. The broad band at 3450 cm^{-1} corresponds to the –OH stretching region of adsorbed water on the surface of goethite [27]. The intensity of this band is much higher in the case of FeNa100 compared to FeNH100, which indicate that the first has more adsorbed water on its surface.

FeNa100 and FeNH100 were subjected to thermogravimetric analysis (TG) and differential thermal analysis (DTA) to study their thermal behavior and to determine the calcination temperature suitable for the formation of iron oxide in each case. The TGA–DTA curves of FeNa100 and FeNH100 are shown in Fig. 2a, b, respectively. As shown in Fig. 2a, the TGA curve of FeNa100 sample exhibits three distinct mass loss steps (at 50–185, 200–280 and 300–400 °C) with three corresponding endothermic DTA peaks (at 73, 216 and 364 °C). The first step (weight loss = 8.1%) can be attributed to the removal of physically adsorbed water, while the second and third steps (total weight loss = 8.5%) can be attributed to the dehydroxylation of goethite to hematite [28–30]. The dehydroxylation of goethite in two steps is consistent with the literature data and reflects the high crystallinity as reported by Liu et al. [29–31]. According to Liu, low crystallinity leads to a complete transformation to hematite before the change of unit cell size, while high crystallinity results in the change in unit cell size and occurs at a higher temperature, which split the dehydroxylation peak into two peaks. Like FeNa100, the TG curve of FeNH100 sample exhibits three mass loss steps (at 50–120, 130–250, and 250–450 °C) with three corresponding DTA peaks (at 98, 240, and 400 °C). The first step (weight loss = 3.6%) which has a corresponding endothermic DTA peak can be attributed to desorption of physically adsorbed water. The amount of adsorbed water in the case of FeNH100 is lower than that in the case of FeNa100, which is in accordance with the FT-IR results. The second and third steps (total mass

loss = 21.2%) that have two corresponding exothermic DTA peaks can be attributed to the dehydroxylation of goethite to hematite [28–30]. The high value of the total mass loss in the second and third steps in the case of FeNH100 and the appearance of exothermic DTA peaks instead of endothermic is likely due to the exothermic decomposition of ammonium nitrate adsorbed on this sample from the mother solution.

The elemental composition of the tin cans used in this study and the prepared iron oxides were assessed by EDAX analysis and presented in Fig. 3a. which shows the EDAX analysis of the used steel can, consisting mainly of iron as it had 89.024% of Fe, 10.54% of Sn, and 0.5% of other elements (Mn, Cr, P, S). Figure 3b, c shows the EDX analysis of FeNa400 and FeNH400, respectively. The weight percentages of Fe in the two oxides are higher than 98.5%. The increase in the weight percentages of Fe at the expense of Sn in the two oxides can be attributed to the preparation method. Iron reacts with nitric acid, forming soluble ferric nitrate ($Fe(NO_3)_3$) while tin reacts with nitric acid, forming insoluble tin oxide (SnO_2) which is removed during the filtration process [32]. The following mechanism can illustrate this process [32]:

$$Sn + 4HNO_3 \rightarrow SnO_3 + 4NO_2 + 2H_2O, \quad (2)$$

$$Fe + 6HNO_3 \rightarrow Fe(NO_3)_3 + 3NO_2 + 3H_2O. \quad (3)$$

Figure 4a, b shows the XRD and FT-IR analysis, respectively, of FeNa400, FeNa500, FeNa600, FeNH400, and FeCm. From Fig. 4a, all the XRD patterns correspond to hematite α-Fe_2O_3 (Rhombohedral; (ICDD NO. 01-076-4579) with its characteristic peaks at 24.22°, 33.26°, 35.76°, 40.97°, 49.57°, 54.17°, 57.75°, 62.53°, 64.08°, 72.06°, and 75.56° [32, 33]. The appearance of the XRD patterns shows that all the prepared iron oxide catalysts have a good crystallinity, which is slightly improved by increasing the calcination temperature in the case of FeNa catalysts. As shown

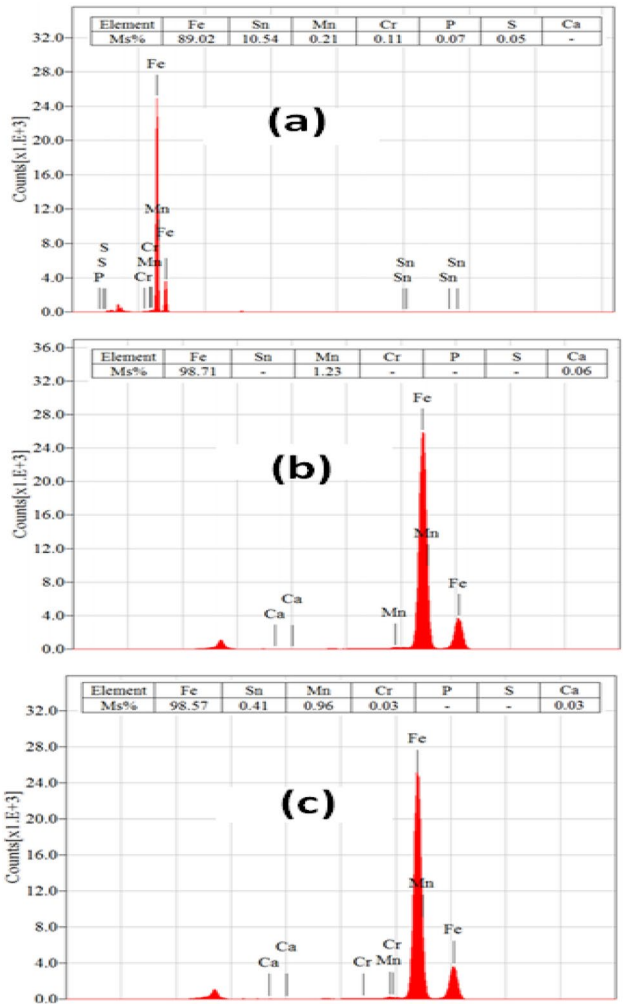

Fig. 3 EDAX analysis of tin food can waste (**a**) and two prepared iron oxide samples, FeNa400 (**b**) and FeNH400 (**c**), after calcination at 400 °C for 2 h in static air

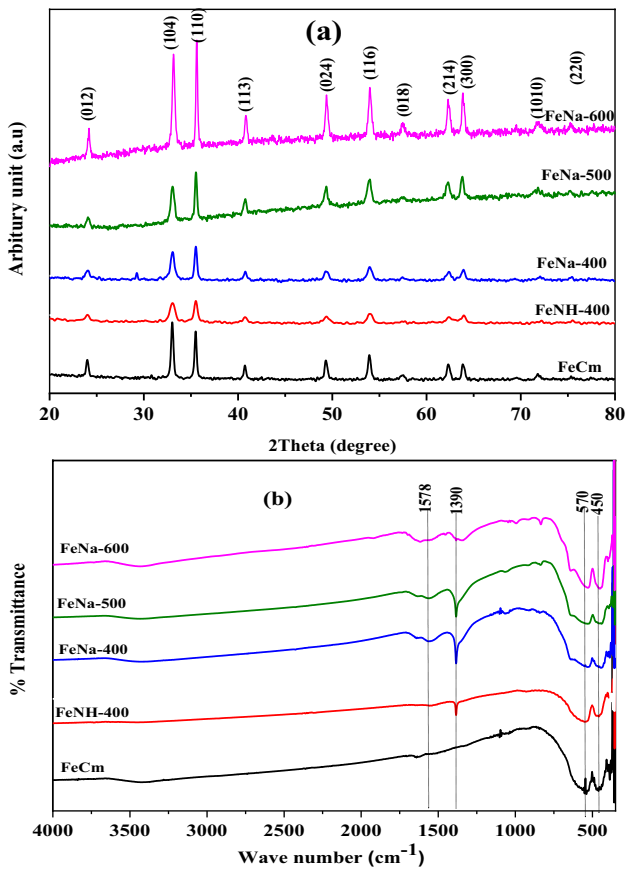

Fig. 4 XRD diffractograms and FT-IR spectra of iron oxide catalysts after calcination at different temperatures 400, 500, and 600 °C, and commercial iron oxide sample

Table 1 Crystallite size (nm), total S_{BET} (m^2/g), micro pore area (m^2/g), and distribution of basic sites (site/g) for iron oxide samples

% SBS[c]	MBS[b]%	% WBS[a]	Total basic sites (site/g)	Micro pore area (m^2/g)	Total S_{BET} (m^2/g)	Crystallite size (nm)	Sample
37.9	40.9	21.2	2.886×10^{20}	2.609	48.73	22.45	FeNH-400
12.7	39.3	47.9	4.299×10^{20}	11.633	49.56	26.30	FeNa-400
17	37	46	4.646×10^{20}	10.684	40.75	31.81	FeNa-500
8.5	51.3	40.2	4.834×10^{20}	5.677	30.78	34.17	FeNa-600
27.7	37.9	34.4	0.927×10^{20}	0.985	13.42	36.50	FeCM

[a]Weak basic sites

[b]Medium basic sites

[c]Strong basic sites

in Table 1, the average crystallite sizes calculated from the XRD patterns, using Scherrer equation are 26.30 nm for FeNa400, 31.81 nm for FeNa500, 34.17 nm for FeNa600, 22.45 nm for FeNH400, and 36.50 nm for FeCm, which indicates that the catalysts are all nanocrystalline. Figure 4b shows the FT-IR spectra of FeNa400, FeNa500, FeNa600, FeNH400, and FeCm samples. The bands located at 450 and 570 cm^{-1} are due to the Fe–O bond vibration in α-Fe_2O_3 [32, 33]. The bands at 1390 and 1578 cm^{-1} correspond to the unidentate adsorbed carbonate group (C=O) resulting from the adsorption of atmospheric carbon dioxide. These two bands are stronger in the case of FeNa400, FeNa500, and FeNa600 samples which may indicate their higher basicity, compared to the other samples [25, 26].

To study the morphology of the catalysts under investigation, SEM images were applied. Figure 5 shows the SEM images of the prepared iron oxide catalysts with a magnification of 3,50,000. We can see that the surface images of FeNa400 and FeNH400 catalysts are quite different from each other, which reflects the effect of the precipitating

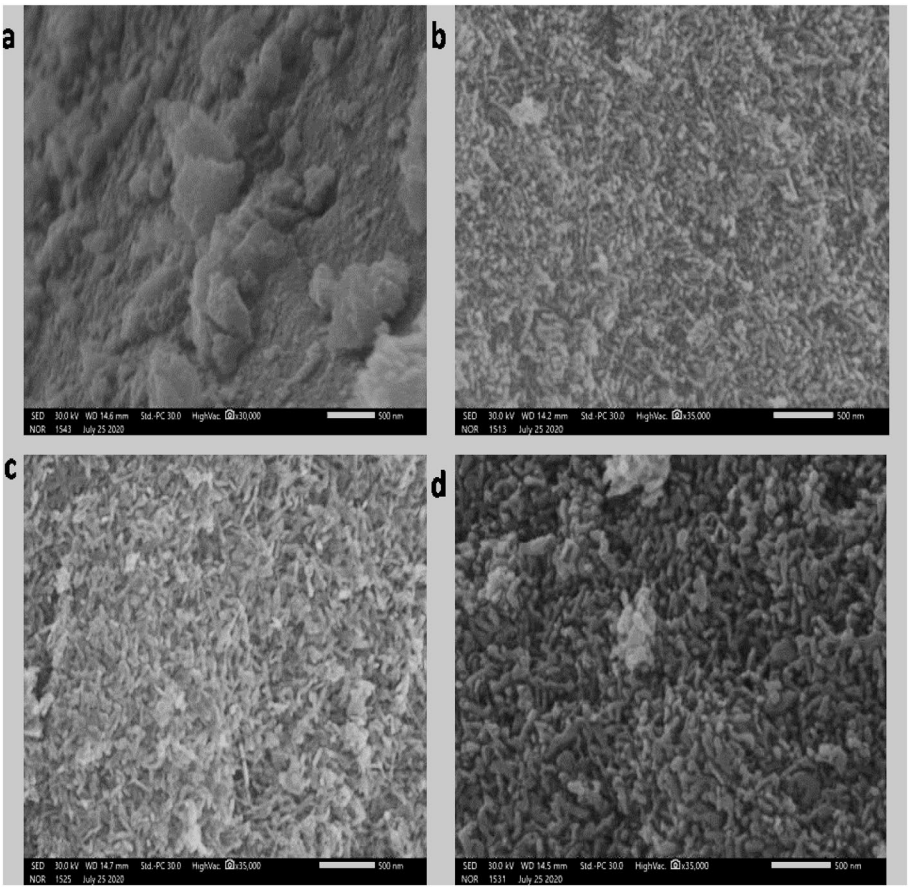

Fig. 5 SEM images of FeNH400 (**a**), FeNa400 (**b**), FeNa500 (**c**), and FeNa600 (d) at 3,50,000 magnification

agents. The image of FeNa400 shows a worm-like morphology with particle size of 27–35 nm, while the image of FeNH400 shows aggregates of particles with irregular shapes and different sizes in the range of 107–155 nm. The catalysts FeNa500 and FeNa600 have the same appearance as that of FeNa400 with a slight increase in the particle size on increasing the calcination temperature, which is likely due to particle agglomeration [34]. The differences between the crystallite or grain sizes measured by XRD and the particle sizes measured by SEM can be attributed to grain agglomeration [35].

The total surface area and micro pore area of all the catalysts under investigation are shown in Table 1. All the prepared iron oxide catalysts have higher surface area than commercial iron oxide. There is no significant effect of the precipitating agent on the surface area of FeNa400 and FeNH400, as the total surface area is almost the same. However, a notable decrease in the micro pore area is observed in the case of FeNH400 catalyst, which is likely because of the formation of large pores due to the collapse of small pores. This can be attributed to the liberation of gases during the decomposition of ammonium nitrate adsorbed on the goethite surface from the mother solution [36]. The effect of increasing the calcination temperature on the surface area and micro pore area is noticeable. With increasing calcination temperature from 400 to 600 °C, the specific surface area of FeNa catalysts decreased from 49.56 to 30.78 m^2/g and the pore area decreased from 11.63 to 5.67 m^2/g which is expected due to solid aggregation [34, 36, 37].

To determine the number of surface basic sites of the prepared and commercial iron oxide catalysts, TG desorption of CO_2 was studied for all catalysts under investigation. The amount of CO_2 desorbed at a given temperature range provides the concentration of basic sites, and the data of total number of basic sites for all catalysts calculated using Eq. (1) are given in Table 1 [38]. The precipitating agent has a strong effect on the surface basicity of the prepared catalysts. The number of basic sites over the surface of FeNa400 catalyst is about 1.5 times that over the surface of FeNH400 catalyst, which is compatible with the FT-IR results of goethite samples. The different amounts of basic sites over the two catalysts may be attributed to different pH values of the precipitate's mother solution in the two cases. The pH value of the mother solution in case of the FeNa400 catalyst is 11.2 (strong basic), while in the case of the FeNH400 catalyst it is 8.18 (weak basic). The effect of mother liquor's pH on the surface acidic–basic properties has been reported previously. Lee and his co-workers [39] reported a decrease in the amount of surface acidic sites by increasing the pH value of the mother solution during the preparation of catalysts by the co-precipitation method. There is no significant effect of calcination temperature of FeNa catalysts on the number of surface basic sites, except for a slight increase when increasing the calcination temperature. The number of basic sites over the surface of the FeCm catalyst is very small compared to all the prepared Fe_2O_3 catalysts.

Catalytic activity

All the prepared iron oxide catalysts along with the commercial iron oxide catalyst were examined in the dehydrogenation of secondary butanol to methyl ethyl ketone as indicated in scheme 1 in the supplementary material. The reaction was carried out in a continuous flow fixed-bed reactor under atmospheric pressure at reaction temperature range of 300–375 °C. Figure 6 shows the conversion of 2-butanol and the selectivity to MEK as a function of reaction temperature over FeNa400, FeNH400, and FeCm. For all catalysts, the increase in the reaction temperature is accompanied by a gradual increase in the % conversion of 2-butanol, due to the fact that the increase in kinetic energy of the reactant molecules enhances their interaction and, consequently, leads to an increase in the conversion of reactants to products [40].

In addition, increasing the reaction temperature activates the active sites over the catalyst surface, which consequently increases the % conversion of 2-butanol [34, 38]. The selectivity to MEK seems to be stable with reaction temperature over all catalysts except for a slight decrease at reaction temperatures higher than 350 °C. The catalyst FeNa400 shows 2-butanol conversion of 54.3% at 300 °C and 96.5% at 375 °C with an average selectivity to MEK of about 96.3%, while the catalyst FeNH400 shows 2-butanol conversion of 47.1% at 300 °C and 93.3% at 375 °C with an average selectivity to MEK of about 85.8%. The commercial iron oxide (FeCm) shows 2-butanol conversion of 37.5% at 300 °C and 83.1% at 375 °C and its average

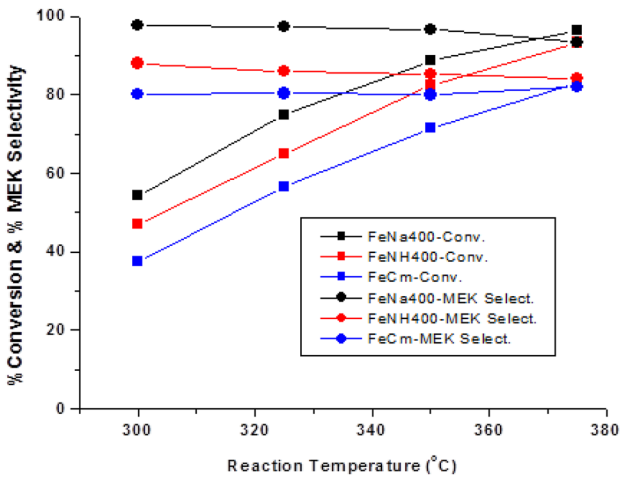

Fig. 6 Conversion of 2-butanol and selectivity to MEK as a function of reaction temperature over FeNa400, FeNH400, and FeCm catalysts (WHSV = 30 L h^{-1} g^{-1})

selectivity to MEK was about 80.7%. So that, the catalytic activity of the three samples toward 2-butanol conversion and MEK selectivity takes the following order: FeNa400 > FeNH400 > FeCm. These results confirm the superiority of the prepared catalysts over the commercial catalyst and the effect of using different precipitating agents on the activity of the prepared iron oxide catalysts. These differences in the catalytic activity between the three catalysts can be attributed to two important factors. The first factor is the surface area over which the reaction occurs, and the second factor is the number of basic sites which are responsible for dehydrogenation of 2-butanol to MEK [38]. The superiority of the prepared catalysts over the commercial catalyst can be attributed to their high surface area and high number of surface basic sites compared to the commercial catalyst. In addition, even though FeNa400 and FeNH400 catalysts have relatively similar surface area, the first exhibits higher catalytic activity and higher selectivity to MEK which can be attributed to its higher surface basicity of about 1.5 times that of FeNH400, see Table 1. The effects of calcination temperature on the catalytic activity of Fe_2O_3 catalysts prepared using NaOH as precipitating agent are shown in Fig. 7. As shown in Fig. 7, the catalytic activity of the three catalysts toward 2-butanol conversion takes the following order: FeNa500 ≥ FeNa400 > FeNa600, while selectivity to MEK is relatively the same over the three catalysts. It can be seen from Table 1 that the number of surface basic sites slightly increases by increasing the calcination temperature from 400 to 600 °C, which explains the relative stability of the selectivity to MEK; however, the surface area decreased in the same direction. The combination between these two factors moving in two opposite directions seems to be optimum with the catalyst FeNa500. Then, 2-butanol conversion decreased over the

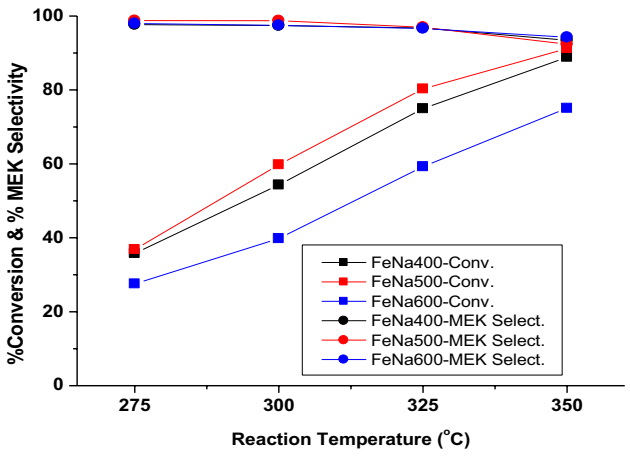

Fig. 7 Conversion of 2-butanol and selectivity to MEK as a function of reaction temperature over FeNa400, FeNa500, and FeNa600 catalysts (WHSV = 30 L h^{-1} g^{-1})

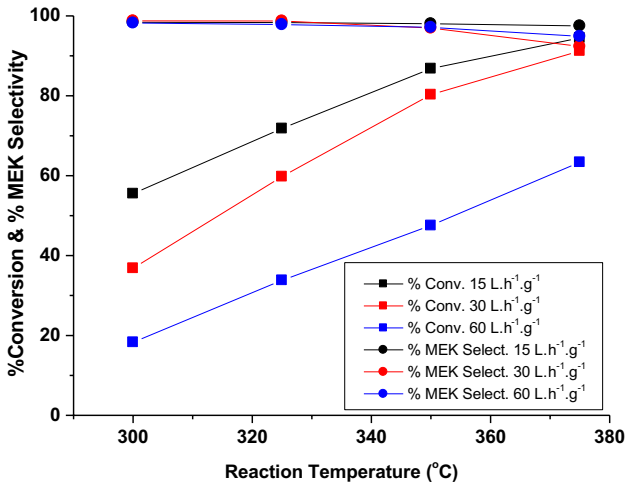

Fig. 8 Conversion of 2-butanol and selectivity to MEK as a function of reaction temperature over FeNa500 catalyst at different values of WHSV

catalysts with higher or lower calcination temperatures. Figure 8 shows the effect of weight hourly space velocity (WHSV) on the catalytic activity and selectivity to MEK over the catalyst FeNa500. which has been chosen for this test as the most active catalyst. WHSV is the mass flow rate of the reactants divided by the mass of the catalyst in the reactor [41, 42]. Three different values of WHSV were applied (i.e., 15, 30 and 60 L h^{-1} g^{-1}) at a temperature range of 275–375 °C. As seen from Fig. 8, by increasing the WHSV from 15 to 30 L. h^{-1} g^{-1}, a slight decrease in the 2-butanol conversion is observed, while further increase of WHSV to 60 L h^{-1} g^{-1} caused a sharp decrease in 2-butanol conversion. This decrease in the value of % conversion of 2-butanol can be attributed to the decrease in the contact time between the reacting molecules and surface-active sites. The higher the value of WHSV, the shorter will be the residence time of the reacting molecules in the reactor, and consequently, the shorter will be the contact time between the reacting molecules and surface-active sites [38, 43]. No effect of changing WHSV on the selectivity to MEK as it is higher than 95% in all cases.

The catalytic activity of the best catalyst in the present study, toward 2-butanol dehydrogenation in terms of 2-butanol conversion as well as selectivity to MEK, was compared with some other catalysts reported in the literature and the values are given in Table 2. Despite the relatively higher reaction temperature used in this study compared with most published studies on this reaction, the importance of this research lies in the facile cost-effective preparation method of the catalyst using cheaply available resources. Furthermore, unlike the most common catalysts used for this

Table 2 Comparison of catalytic activity of the prepared iron oxide with other commonly used catalysts toward 2-butanol dehydrogenation

Catalyst	Temperature range (°C)	Maximum 2-butanol conversion (%)	Maximum MEK selectivity (%)	Refs.
FeNa500	375	93.0	94.9	This study
NiO	325	96.1	92.5	[20]
$CuO–ZnO/Al_2O_3–ZrO_2$	260	95.0	78.0	[19]
CuO/SiO_2 (sol–gel)	260	92.2	89.0	[15]
CuO/SiO_2 (impregnation)	260	77.2	44.1	[15]
$CuO/ZnO/Al_2O_3$	260	93.1	90.3	[15]
ZnO	350	78.9	95.9	[46]
$1\%K_2O/ZnO$	350	99.8	97.3	[46]
NiO	275	76.8	98.2	[38]
10%F/NiO	275	99.3	98.0	[38]
$1\%K_2O/NiO$	275	95.0	95.9	[38]

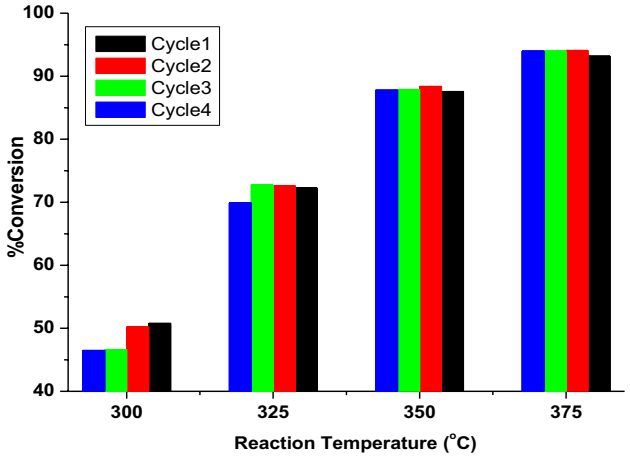

Fig. 9 Conversion of 2-butanol as a function of reaction temperature in four successive cycles over FeNa500 catalyst

reaction, iron oxide is a safe non-hazardous material which makes it environmentally favorable.

Catalyst stability and reusability

Long-term stability and reusability represent one of the most important and essential properties that make the catalyst suitable for industrial large-scale application [44, 45]. To examine the catalytic stability and reusability of FeNa500 catalyst, four complete cycles of the reaction were carried out at the temperature range of 300–375 °C. Each cycle took about 5 h. A refreshment step was applied before each new cycle, involving heating the catalyst at 400 °C for 1 h in a flow of nitrogen. After four cycles, the catalyst exhibited stability in both of 2-butanol conversion and selectivity to MEK, with the only exception being a slight decrease in the % conversion of 2-butanol starting from the third cycle at a low reaction temperature (i.e., 300 °C) as shown in Fig. 9. Therefore, we strongly recommend the FeNa500 catalyst as a promising low-cost, environmentally friendly, and available catalyst for the production of MEK from 2-butanol. It is important to note that this method of testing the stability and reusability of catalysts has been previously applied to study the stability and reusability for different catalysts [34, 38].

Conclusion

Iron oxide catalysts were prepared from tin food cans by the simple precipitation method using sodium hydroxide and ammonium hydroxide as two different precipitating agents. The catalytic efficiency of the prepared iron oxide catalysts was tested in the dehydrogenation reaction of 2-butanol to MEK. The precipitating agent clearly affects the morphology and surface properties of the produced iron oxide, and accordingly, the catalytic properties toward 2-butanol dehydrogenation were affected. Using NaOH as precipitating agent produces iron oxide with higher density of surface basic sites compared to that prepared using NH_4OH as precipitating agent, which is likely related to the pH of the mother solution in both cases. The catalyst prepared using NaOH as a precipitating agent and calcined at 500 °C shows the best catalytic efficiency compared to the other catalysts in this study. All the prepared catalysts in this study exhibited high catalytic activity toward the test reaction, compared to the commercial iron oxide catalyst under the same reaction conditions. Iron oxide catalysts recovered from tin food can waste can be considered as promising low-cost, basic solid catalysts for the production of MEK from 2-butanol.

Supplementary Information The online version contains supplementary material available at https://doi.org/10.1007/s10163-023-01865-8.

Funding Open access funding provided by The Science, Technology & Innovation Funding Authority (STDF) in cooperation with The Egyptian Knowledge Bank (EKB).

References

1. Nanda S, Berruti F (2021) Municipal solid waste management and landfilling technologies: a review. Environ Chem Lett 19(2):1433–1456
2. Zorpas AA, Navarro-Pedreño J, Jeguirim M, Dimitriou G, Almendro Candel MB, Argirusis C, Papamichael I (2021) Crisis in leadership vs waste management. Euro-Mediterr J Environ Integr 6(3):1–5
3. Ruj B, Ghosh S (2014) Technological aspects for thermal plasma treatment of municipal solid waste. A review. Fuel Process Technol 126:298–308
4. Suthar S, Singh P (2015) Household solid waste generation and composition in different family size and socio-economic groups: a case study. Sustain Cities Soc 14:56–63
5. Sondh S, Upadhyay DS, Patel S, Patel RN (2022) A strategic review on municipal solid waste (living solid waste) management system focusing on policies, selection criteria and techniques for waste-to-value. J Clean Prod 365:131908
6. Khan AH, López-Maldonado EA, Khan NA, Villarreal-Gómez LJ, Munshi FM, Alsabhan AH, Perveen K (2021) Current solid waste management strategies and energy recovery in developing countries—state of art review. Chemosphere 291:133088
7. Lin K, Zhao Y, Kuo JH, Deng H, Cui F, Zhang Z, Wang T (2022) Toward smarter management and recovery of municipal solid waste: a critical review on deep learning approaches. J Clean Prod 346:130943
8. Liu C, Sun S, Zhu X, Tu G (2021) Feasibility of platinum recovery from waste automotive catalyst with different carriers via cooperative smelting-collection process. J Mater Cycles Waste Manage 23:581–590
9. Marinato Y, Pavoski G, Rosario CGA, de Andrade LM, Espinosa DCR (2023) Ag recovery from waste printed circuit boards of cell phone for synthesis of Ag nanoparticles and their antibacterial activity. J Mater Cycles Waste Manage 25(2):970–984
10. Wang WY, Yen CH, Lin JL, Xu RB (2019) Recovery of high-purity metallic cobalt from lithium nickel manganese cobalt oxide (NMC)-type Li-ion battery. J Mater Cycles Waste Manage 21:300–307
11. Roy K, Sikdar D, Pongwisuthiruchte A, Debnath SC, Potiyaraj P (2022) Application of waste aluminum cans based nano alumina as reinforcing filler in natural rubber composites. J Mater Cycles Waste Manage 24(4):1533–1541
12. Blunden S, Wallace T (2003) Tin in canned food: a review and understanding of occurrence and effect. Food Chem Toxicol 41(12):1651–1662
13. Sánchez-Ramírez E, Alcocer-García H, Romero-García AG, Contreras-Zarazua G, Segovia-Hernandez JG (2021) Improvements in methyl ethyl ketone production through intensified processes. Comput Aided Chem Eng 50:399–405
14. Zhenhua LIU, Wenzhou HUO, Hao MA, Kai QIAO (2006) Development and commercial application of methyl-ethyl-ketone production technology. Chin J Chem Eng 14(5):676–684
15. Geravand E, Shariatinia Z, Yaripour F, Sahebdelfar S (2015) Synthesis of copper–silica nanosized catalysts for 2-butanol dehydrogenation and optimization of preparation parameters by response surface method. Chem Eng Res Des 96:63–77
16. Ndaba B, Chiyanzu I, Marx S (2015) n-butanol derived from biochemical and chemical routes: a review. Biotechnol Rep 8:1–9
17. Fang D, Ren W, Liu Z, Xu X, Xu L, Lü H, Zhang H (2009) Synthesis and applications of mesoporous Cu–Zn–Al_2O_3 catalyst for dehydrogenation of 2-butanol. J Nat Gas Chem 18(2):179–182
18. Mitran G, Saab R, Charisiou N, Polychronopoulou K, Goula M (2020) Molybdenum supported on carbon covered alumina: active sites for n-butanol dehydrogenation and ketonization. Mol Catal 495:111159
19. Zhang L, Jiang M, Zhang Y (2023) Preparation of Al_2O_3–ZrO_2 composite carrier catalyst and its application in the dehydrogenation reaction of 2-butanol. Russ J Phys Chem 97(4):603–609
20. Halawy SA, Mohamed MA, Abdelkader A (2018) Hierarchical nanocrystalline NiO with coral-like structure derived from nickel galactarate dihydrate: an active mesoporous catalyst for methyl ethyl ketone production. Arab J Chem 11(6):991–999
21. Mishra M, Chun DM (2015) α-Fe_2O_3 as a photocatalytic material: a review. Appl Catal A 498:126–141
22. Osman AI, Abu-Dahrieh JK, Rooney DW, Halawy SA, Mohamed MA, Abdelkader A (2012) Effect of precursor on the performance of alumina for the dehydration of methanol to dimethyl ether. Appl Catal B 127:307–315
23. Namgung S, Guo B, Sasaki K, Lee SS, Lee G (2020) Macroscopic and microscopic behaviors of Mn (II) adsorption to goethite with the effects of dissolved carbonates under anoxic conditions. Geochim Cosmochim Acta 277:300–319
24. Encina ER, Distaso M, Klupp Taylor RN, Peukert W (2015) Synthesis of goethite α-FeOOH particles by air oxidation of ferrous hydroxide $Fe(OH)_2$ suspensions: Insight on the formation mechanism. Cryst Growth Des 15(1):194–203
25. Dash B, Dash B, Rath SS (2020) A thorough understanding of the adsorption of Ni(II), Cd(II) and Zn(II) on goethite using experiments and molecular dynamics simulation. Sep Purif Technol 240:116649
26. Godwin J, Abdus-Salam N, Haleemat AI, Panda PK, Panda J, Tripathy BC (2022) Facile synthesis of rod-like α-FeOOH nanoparticles adsorbent and its mechanism of sorption of Pb(II) and indigo carmine in batch operation. Inorg Chem Commun 140:109346
27. Salama W, El Aref M, Gaupp R (2015) Spectroscopic characterization of iron ores formed in different geological environments using FT-IR, XPS, Mossbaur spectroscopy and thermoanalysis. Spectrochim Acta A Mol Biomol Spectrosc 136:1816–1826
28. Ponomar VP (2018) Thermomagnetic properties of the goethite transformation during high-temperature treatment. Miner Eng 127:143–152
29. Faris N, Tardio J, Ram R, Bhargava S, Pownceby MI (2017) Investigation into coal-based magnetizing roasting of an iron-rich rare earth ore and the associated mineralogical transformations. Miner Eng 114:37–49
30. Christensen AN, Jensen TR, Bahl CR, DiMasi E (2007) Nano size crystals of goethite, α-FeOOH: synthesis and thermal transformation. J Solid-State Chem 180(4):1431–1435

31. Frost RL, Ding Z, Ruan HD (2003) Thermal analysis of goethite. J Therm Anal Calorim 71(3):783–797
32. Abdelrahman EA, Hegazey RM, Kotp YH, Alharbi A (2019) Facile synthesis of Fe_2O_3 nanoparticles from Egyptian insecticide cans for efficient photocatalytic degradation of methylene blue and crystal violet dyes. Spectrochim Acta A Mol Biomol Spectrosc 222:117195
33. Onizuka T, Iwasaki T (2022) Low-temperature solvent-free synthesis of polycrystalline hematite nanoparticles via mechanochemical activation and their adsorption properties for Congo red. Solid State Sci. https://doi.org/10.1016/j.solidstatesciences.2022.106917
34. Gomaa AA, Halawy S, Abdelkader A (2021) Preparation and characterization of nanocrystalline NiO by the thermal decomposition of oxalate salts for the dehydrogenation of 2-butanol to methyl ethyl ketone. Aswan Univ J Environ Stud 2(3):178–189
35. Graeve OA, Madadi A, Kanakala R, Sinha K (2010) Analysis of particle and crystallite size in tungsten nanopowder synthesis. Metall Mater Trans A 41(10):2691–2697
36. Barik R, Jena BK, Dash A, Mohapatra M (2014) In situ synthesis of flowery-shaped α-FeOOH/Fe_2O_3 nanoparticles and their phase dependent supercapacitive behaviour. RSC Adv 4(36):18827–18834
37. Kusuma M, Chandrappa GT (2019) Effect of calcination temperature on characteristic properties of $CaMoO_4$ nanoparticles. J Sci Adv Mater Devices 4(1):150–157
38. Halawy SA, Osman AI, Abdelkader A, Yang H (2021) Boosting NiO catalytic activity by x wt% F-ions and K_2O for the production of methyl ethyl ketone (MEK) via catalytic dehydrogenation of 2-butanol. ChemCatChem 13(9):2200–2214
39. Lee H, Jung JC, Kim H, Chung YM, Kim TJ, Lee SJ, Oh SH, Kim YS, Song IK (2008) Preparation of $ZnFe_2O_4$ catalysts by a co-precipitation method using aqueous buffer solution and their catalytic activity for oxidative dehydrogenation of n-butene to 1, 3-butadiene. Catal Lett 122(3):281–286
40. Castelo-González OA, Sotelo-Lerma M, García-Valenzuela JA (2017) Effect of reaction time and temperature on chemical, structural, optical, and photoelectrical properties of PbS thin films chemically deposited from the Pb $(OAc)_2$–NaOH–TU–TEA aqueous system. J Electron Mater 46(1):393–400
41. Nagaraju N, Kumar VP, Srikanth A, Rajan NP, Chary KV (2016) Vapor-phase catalytic dehydration of lactic acid to acrylic acid over nano-crystalline cerium phosphate catalysts. Appl Petrochem Res 6(4):367–377
42. Fortunate O, Kishore N (2021) Computational fluid dynamics investigation on catalytic hydrodeoxygenation of a bio-oil model compound in a fluidized bed reactor. J Therm Sci Eng Appl 5:100287
43. Natesakhawat S, Means NC, Howard BH, Smith M, Abdelsayed V, Baltrus JP, Cheng Y, Lekse JW, Link D, Morreale BD (2015) Improved benzene production from methane dehydroaromatization over Mo/HZSM-5 catalysts via hydrogen-permselective palladium membrane reactors. Catal Sci Technol 5(11):5023–5036
44. Singh B, Sharma V, Gaikwad RP, Fornasiero P, Zboril R, Gawande MB (2021) Single-atom catalysts: a sustainable pathway for the advanced catalytic applications. Small 17(16):2006473
45. Huang Y, Zhang W, Yue Z, Zhao X, Cheng Z (2017) Performance of SiO_2–TiO_2 binary oxides supported Cu–ZnO catalyst in ethyl acetate hydrogenation to ethanol. Catal Lett 147(11):2817–2825
46. Halawy SA, Osman AI, Rooney DW (2022) Highly basic and active ZnO–x% K_2O nanocomposite catalysts for the production of methyl ethyl ketone biofuel. Energy Sci Eng 10(8):2827–2841

Authors and Affiliations

Abouelhassan A. Gomaa[1] · Ahmed I. Osman[2] · Samih A. Halawy[1] · Mohamed A. Mohamed[1] · Adel Abdelkader[1]

✉ Adel Abdelkader
adel.abdelkader@sci.svu.edu.eg

[1] Nanocomposite Catalysts Lab., Chemistry Department, Faculty of Science at Qena, South Valley University, Qena 83523, Egypt

[2] School of Chemistry and Chemical Engineering, Queens University Belfast, David Keir Building, Belfast BT95AG, Northern Ireland, UK